Title	Correlation between dry etching resistance of Ta masks and the oxidation states of the surface oxide layers
Author(s)	Satake, Makoto; Yamada, Masaki; Li, Hu et al.
Citation	Journal of Vacuum Science and Technology B: Nanotechnology and Microelectronics. 2015, 33(5), p. 051810
Version Type	VoR
URL	https://hdl.handle.net/11094/78463
rights	This article may be downloaded for personal use only. Any other use requires prior permission of the author and AIP Publishing. This article appeared in Journal of Vacuum Science & Technology B 33, 051810 (2015) and may be found at https://doi.org/10.1116/1.4930242.
Note	

Correlation between dry etching resistance of Ta masks and the oxidation states of the surface oxide layers

Makoto Satake, Masaki Yamada, Hu Li, Kazuhiro Karahashi, and Satoshi Hamaguchi

View Online   Export Citation   CrossMark

Correlation between dry etching resistance of Ta masks and the oxidation states of the surface oxide layers

Makoto Satake[a)]
Central Research Laboratory, Hitachi, Ltd., 1-280, Higashi-koigakubo, Kokubunji-shi, Tokyo 185-8601, Japan and Center for Atomic and Molecular Technologies, Graduate School of Engineering, Osaka University, 2-1 Yamadaoka, Suita, Osaka 565-0871, Japan

Masaki Yamada
Central Research Laboratory, Hitachi, Ltd., 1-280, Higashi-koigakubo, Kokubunji-shi, Tokyo 185-8601, Japan

Hu Li, Kazuhiro Karahashi, and Satoshi Hamaguchi
Center for Atomic and Molecular Technologies, Graduate School of Engineering, Osaka University, 2-1 Yamadaoka, Suita, Osaka 565-0871, Japan

Mechanisms of dry etching resistance of Ta masks, which are widely used for magnetic random access memory etching processes, have been investigated for a better understanding of their faceting characteristics. In magnetic-material etching processes by CO/NH_3 or CH_3OH plasmas, CO^+ ion is considered as one of the most dominant ion species irradiating the substrate surface. An earlier study by Li *et al.* [J. Vac. Sci. Technol. A **33**, 040602 (2015)] has shown that the Ta sputtering yield by CO^+ ion irradiation depends strongly on the ion irradiation angle and the level of the surface oxidation. In this study, the primary focus is placed on the effects of surface oxidation and physical sputtering only (without possible chemical effects of carbon) on the etching rate of Ta, and the etching characteristics of Ta and Ta_2O_5 have been examined with Ar^+ and/or oxygen ion beams. It has been found that there is a strong negative correlation between the etching rate of Ta and the oxidation states of the surface oxide layer formed during the etching process; the higher the oxidation states are, the lower the etching rate becomes. The results indicate that a strong propensity of a Ta mask to taper by irradiation of oxidizing ions (i.e., strong ion-irradiation-angle dependence of the Ta etching rate) arises from less efficient oxidation of a tapered surface by incident oxidizing ions, which enter the surface with an oblique angle. © 2015 American Vacuum Society. [http://dx.doi.org/10.1116/1.4930242]

I. INTRODUCTION

Magnetic random access memory (MRAM) is considered to be one of the most promising candidates for the next generation memory technologies because of its nonvolatility, fast reading and writing speed, and high write-cycle endurance.[1,2] Especially with the spin-transfer torque MRAM technology,[3–8] the write current of the device may be further reduced, and therefore, the scaling limit of the earlier MRAMs may be overcome. To establish successful MRAM commercial fabrication technologies, however, a high-density integration of MRAM devices must be achieved, which necessitates the development of nanoscale anisotropic etching technologies for magnetic materials.

Plasma etching of magnetic materials such as CoFeB, NiFe, and PtMn has been extensively studied with plasmas of CO/NH_3 or CH_3OH gases.[9–18] The advantages of these processes include no corrosion of magnetic materials during the process and high etching selectivity of hard mask materials such as Ta, Ti, and TiN over magnetic materials. Matsui *et al.*[12] pointed out that the high mask selectivity was due to the formation of a hardening surface layer on the mask by nitridation, carbonization, or oxidation. In the previous studies of Ref. 19, x-ray photoelectron spectroscopy (XPS) analysis of Ni and Ta surfaces irradiated by CO^+ ions revealed that an oxide layer was formed only on the Ta surface (and not on the Ni surface) and a high etching selectivity of Ni over Ta was attained. Although it has been known that the physical sputtering yield of Ni is higher than that of Ta in general,[20] the oxidation of Ta may further suppress its etching rate and the observed high mask selectivity in CO/NH_3 or CH_3OH plasma may be attributed to the selective oxidation of the mask materials, rather than increased etching rates of the magnetic materials.

In addition, mask faceting poses a critical problem for high density patterning of DRAM devices as mask faceting causes hard mask shrinking. It is known that faceting of a mask structure is caused by a strong angle dependence of the sputtering yield of the mask material.[21–23] A previous study of Ref. 24 shows that the sputtering yield of Ta by energetic CO^+ ions strongly depends on the ion irradiation angle and suggests that the strong angular dependence may be caused by angular dependence of surface oxidation.

The goal of this study is to understand the effects of surface oxidation on Ta etching and the mechanisms of the strong dependence of the Ta etching rate on the ion irradiation angle when the surface is irradiated by energetic oxidizing ions. In CO/NH_3 or CH_3OH plasma processes, the main

etching mechanism of magnetic materials is considered to be physical sputtering[12,16] (rather than chemical sputtering forming volatile metal complexes) and therefore the selectivity should arise from etch resistance of mask materials. In this study, we conjecture that the etch resistance of Ta masks is significantly enhanced when its surface is highly oxidized. Therefore, focusing only on the effects of surface oxidation and physical sputtering (without possible chemical effects of other species such as carbon), we examine the etching characteristics of Ta and Ta_2O_5 primarily using Ar^+ and/or oxygen ion beams.

II. EXPERIMENT

A. Outline of the experiment

In the experiments, Ta and its oxide (Ta_2O_5) films were etched by Ar^+, CO^+, and/or oxygen ion beams and their etching rates, surface chemical compositions, and ion species emitted from the surface were examined in an attempt for us to understand how the dry etching resistance of Ta may be enhanced during magnetic material etching processes. The Ta or Ta_2O_5 films were formed by sputtering deposition in an ultrahigh vacuum sputtering system. More specifically, the Ta film was typically formed on a thin Pt layer deposited on SiO_2 that had been thermally grown on a Si substrate whereas Ta_2O_5 is typically formed directly on a Si substrate. A Pt-cap layer was then formed on each Ta film surface to prevent the surface oxidation due to air exposure. The thickness of each Ta or Ta_2O_5 sample film was precisely known prior to the ion beam etching (IBE) experiments.

In this study, we used three different ion beam systems to irradiate sample surfaces with energetic ions at an incident energy of 500 eV or 1 keV. The first system is a mass-selected ion beam system, in which a sample surface may be irradiated with a mass and energy selected ion beam. The system is equipped with an *in situ* XPS system, which allows analysis of surface chemical compositions of the sample surface after an ion beam irradiation process without exposing the sample to ambient air. The second system is an Ar and O_2 mixture-IBE (Ar/O_2 IBE) system, in which an ion beam is generated in an electron cyclotron resonance (ECR) plasma source. The system is equipped with a secondary ion mass spectroscopy (SIMS) system, which allows *in situ* measurements of the depth profiles of chemical compositions of the sample. In this study, the SIMS system was used to detect ion species emitted from the sample surface (i.e., secondary ions) due to ion irradiation. The third system is an Ar ion gun equipped in a stand-alone XPS system (which is different from the *in situ* XPS system equipped in the mass-selected ion beam system). A sample was placed in this XPS system just as a standard measurement process for any sample. The change in surface chemical compositions of the sample was observed by XPS after its surface was etched by Ar ion irradiation from the ion gun without exposure to ambient air. In what follows, we shall give brief account on each ion beam system and measurements with it.

B. Mass-selected ion beam system

The mass-selected ion beam system used in this study allows ions of specific mass to be injected into a sample surface with specified incident energy.[25–32] In this system, ions are generated in an ion source and specific ions such as Ar^+ or CO^+ relevant for this study are selected by the mass analyzing magnet. Ions thus extracted and selected are then injected into the surface of a sample set in the ultrahigh vacuum chamber, where the gas pressure is typically kept in the range of 10^{-8} Pa. With a rotatable sample holder, the ion incident angle can be varied from 0° (i.e., normal incidence) to about 80°. The ion beam current is measured by a Faraday cup. Details of the ion beam system may be found in Ref. 32.

The sample used in each experiment of this study was a Ta film formed on a 1.5×1.5 cm² square Si substrate. Prior to Ar^+ or CO^+ beam injection, the sample surface was cleaned by 1 keV Ar^+ ion injection. The etching rate is defined as the etched depth achieved per unit time by ion irradiation. The etched depth was measured by a surface profiler (Dektak3ST) after the ion irradiation process was over and the sample was taken outside from the chamber. The ion dose used for etching rate measurements in this system was in the range of 1×10^{17} to 3×10^{18} ions/cm². The chemical compositions of some beam-irradiated sample surfaces were analyzed with an *in situ* XPS system equipped in the mass-selected ion beam system. The ion dose used for the preparation of a sample for XPS observation was approximately 1×10^{17} ions/cm², at which the etching process typically reached steady state.

C. Ar/O_2 IBE system

The Ar/O_2 IBE system is a plasma-based ion beam system equipped with an *in situ* SIMS system, as illustrated in Fig. 1. The system is designed to process 75-mm wafers. The ECR plasma source is operated at 2.45 GHz with a uniform magnetic field of 0.0875 T. A sample wafer is set at the
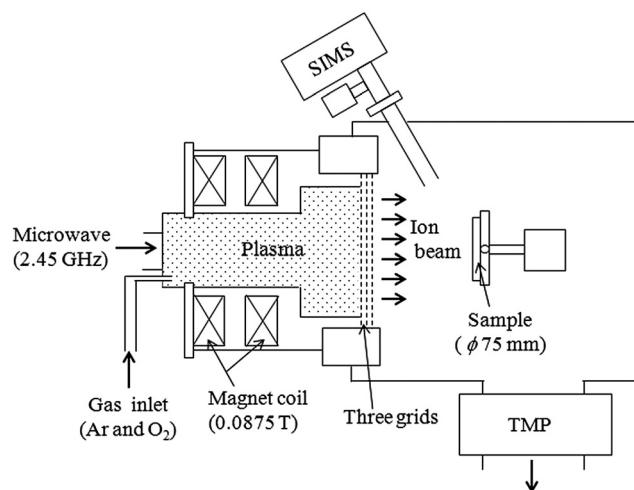

FIG. 1. Schematic illustration of the Ar/O_2 IBE system used in this study. The ion beam energy was set at 500 eV, and the incident ion beam angle was normal to the sample surface.

sample stage and the stage is cooled to 15 °C. In order not to overheat the sample surface by continuous ion irradiation for an extended period, we typically irradiate the sample surface with reasonable intermissions. The process chamber is pumped down by a turbomolecular pump (TMP), and the base pressure of the chamber is typically maintained in the range of 1.9–2.9×10^{-5} Pa.

The ECR plasma source and the process chamber are separated by three grids, i.e., an accelerator grid, a decelerator grid, and a grounded grid. A collimated ion beam is extracted from the plasma source through the three grids and led to the sample material placed on the sample holder. The ion beam energy used in this study with this system was set at 500 eV and the angle of beam incidence (i.e., ion irradiation angle) was normal to the sample surface. The ion current density of the IBE system was approximately 0.7 mA/cm^2. A pure Ar gas or a mixture of Ar and O_2 gas may be supplied to the plasma source, and the gas-flow rate may be controlled to keep the total pressure in the process chamber at a preset value. In this study, the pressure was maintained at 0.53 Pa. During the ion irradiation process, ion species emitted from the sample surface may be monitored by the SIMS system.

The way we evaluated the etching rate using the Ar/O_2 IBE system was different from the way we did using the mass-selected ion beam system discussed above. During an ion beam etching process in the Ar/O_2 IBE system, secondary ions (i.e., ions emitted from the sample surface) are monitored with the *in situ* SIMS system. As the beam etching proceeds, Ta^+ or TaO^+ ions from the Ta or Ta_2O_5 film are observed. (In the case of a Ta sample, Pt^+ ions from the Pt cap are initially observed.) When ions from the underneath layer are observed, we know that the Ta or Ta_2O_5 film is completely removed. From the elapsed time to complete the etching of the Ta or Ta_2O_5 film, whose thickness is known, one can estimate the etching rate.

When a gas mixture of Ar and O_2 is used to generate a plasma, ions extracted from the plasma should consist of Ar^+, O^+, O_2^+, etc. When such an Ar/O_2 mixed ion beam is used to irradiate a Ta film, a thin tantalum oxide (TaO_x) layer is typically formed on the Ta surface. In this study, we evaluated the thickness of a TaO_x layer formed by the irradiation of an Ar/O_2 mixed ion beam for a fixed duration (typically 50 s). The thickness of such an oxide layer was evaluated *in situ* in the following manner: When an oxide layer was formed on the sample Ta surface, the surface was then exposed to a pure Ar ion beam generated in the plasma source. Note that the sample needs not to be taken outside from the vacuum chamber. The SIMS system was used during the Ar^+ ion irradiation to detect secondary ions such as TaO_x^+ emitted from the oxide layer surface and the time that it took for the ion beam to remove the oxide layer completely was evaluated. Assuming the etching rate of the formed oxide (TaO_x) layer was the same as the known etching rate of Ta_2O_5 by a pure Ar^+ ion beam, we estimated the thickness of the formed TaO_x layer.

D. Ar$^+$ ion gun of an XPS system

An Ar^+ ion gun equipped in a theta probe angle-resolved XPS system (Thermo Fisher Scientific) was also used to study the change in chemical compositions of Ta_2O_5 sample surfaces due to Ar^+ ion bombardment. The x-ray of this XPS system was a monochromatic Al Kα emission line. The binding energy of adventitious carbon (C1s at 284.6 eV) was used as a charge reference for the XPS spectra.

III. RESULTS AND DISCUSSION

A. Angle dependent etching rates and surface oxidation of Ta by CO$^+$ ion irradiation

Figure 2 shows the ion-irradiation-angle dependence of the Ta etching rates by Ar^+, CO^+, and O^+ ion irradiation.

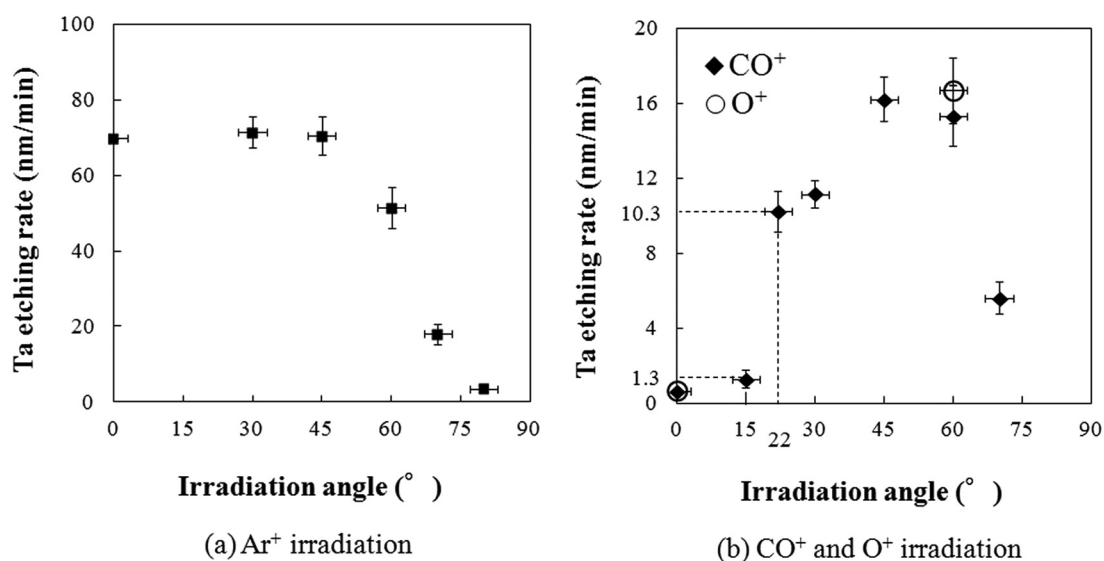(a) Ar$^+$ irradiation

(b) CO$^+$ and O$^+$ irradiation

FIG. 2. Dependence of Ta etching rates on the angle of incidence by (a) Ar$^+$ and (b) CO$^+$ and O$^+$ ion irradiation. The experiments were performed in the mass-selected ion beam system. The data for Ar$^+$ and CO$^+$ ion irradiation here are identical to those given in Fig. 2 of Ref. 24 although they are represented here as the etching rates rather than the sputtering yields given in Ref. 24. The ion incident energy is 1 keV, and the ion dose is in the range of 1×10^{17} to 3×10^{18} ions/cm^2.

The experiments were performed in the mass-selected ion beam system discussed in Sec. II B. The data for Ar$^+$ and CO$^+$ ion irradiation here are identical to those given in Fig. 2 of Ref. 24, although they are represented here as the etching rates rather than the sputtering yields given in Ref. 24. The ion incident energy was 1 keV in all cases, and the ion dose was in the range of 1×10^{17} to 3×10^{18} ions/cm^2.

As mentioned in the Sec. II B, the etched depth of a sample processed in the mass-selected ion beam system was measured by a surface profiler *ex situ*. The etching rate, i.e., the etched depth per unit time, was evaluated from the measured etched depth and beam irradiation time. The corresponding sputtering yields, such as those given in Ref. 24, may be calculated from the etching rates with the knowledge of the ion beam currents measured with a Faraday cup equipped in the mass-selected ion beam system. It should be noted that the etching rate R (i.e., the etched depth per unit time) is proportional to $Y \cdot \cos \theta$ with Y and θ being the sputtering yield and the beam irradiation angle measured from the surface normal. The sputtering yield Y here is defined as the number of sputtered Ta atoms per incident ion.

It is seen in Fig. 2 that the etching rate of Ta by Ar$^+$ ion irradiation is a weak function of the irradiation angle for angles smaller than 45°, whereas the etching rate of Ta by CO$^+$ ions irradiation shows a strong angular dependence, especially at small angles. Furthermore, there is a nearly discontinuous increase of the etching rate of Ta by CO$^+$ ion irradiation as the irradiation angle increases from 15° to 22° (where the etching rate is shown to increase from 1.3 to 10.3 nm/min) With multiple measurements, we have confirmed that this relatively large difference in the etching rate between 15° and 22° is not mere statistical noise.

Since the angular dependence of the Ta etching rate by Ar$^+$ ions is not as strong as that by CO$^+$ ions and Ar$^+$ ion incidence causes only physical sputtering, the strong angular dependence seen in Fig. 2(b) by CO$^+$ ions is most likely caused by some chemical effects of carbon or oxygen of the incident beam. In order to clarify the effects of incident oxygen ions only (without carbon), the etching rates of Ta by O$^+$ ion irradiation (only at 0° and 60°) were measured, as shown in Fig. 2(b). The strong angular dependence of the Ta etching rate was also confirmed by O$^+$ ion irradiation.

The results of Fig. 2(b) suggest that surface oxidation (rather than effects of carbon of incident CO$^+$ ions) affects the etching rate. Figure 3 shows the ion-irradiation-angle dependence of Ta4f spectra of Ta sample surfaces after CO$^+$ ion irradiation, obtained by the *in situ* XPS system equipped in the mass-selected ion beam system. The ion incident energy was 1 keV, and the ion dose was approximately 1×10^{17} cm^{-2}. Reference 24 also presents similar XPS data for Ta4f spectra of Ta after CO$^+$ ion irradiation at incident angles of 0° and 60°. All data presented in Fig. 3 are new and obtained from ion beam irradiation experiments performed in the mass-selected ion beam system at four different beam incident angles.

In the spectra of Fig. 3, Ta^{x+} ($0 \leq x \leq 5$) represents the oxidation state of Ta with Ta^0 being metallic Ta. The thick
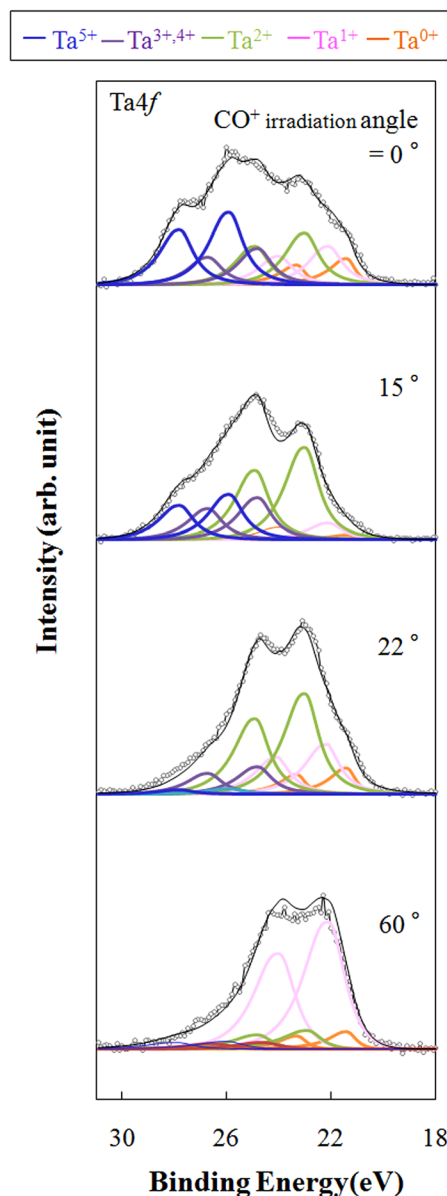

FIG. 3. (Color online) Ta4f spectra measured by XPS for Ta sample surfaces exposed to a CO$^+$ ion beam with angles of incident being 0° (normal incidence), 15°, 22°, and 60°. The experiments were performed in the mass-selected ion beam system and the XPS spectra were taken *in situ*. The oxidation states are represented by Ta^{x+} ($0 \leq x \leq 5$) with Ta^0 being metallic Ta (Ref. 24). The ion incident energy is 1 keV, and the ion dose is approximately 1×10^{17} cm^{-2}.

blue curves represent spectra of Ta^{5+}, i.e., the highest oxidation state of Ta, which suggests the formation of Ta$_2$O$_5$ on the Ta surface. It is clearly seen in Fig. 3 that, at an irradiation angle of 15° or lower, a relatively large amount of Ta^{5+} is formed, whereas, at an irradiation angle of 22° or higher, the Ta sample surface is much more metallic. The change of the oxidation states with the change of the irradiation angle seen in Fig. 3 exhibits some correlation with that of the etching rate presented in Fig. 2(b). The correlation suggests that the formation of an oxide layer with higher oxidation states causes higher etching resistance (i.e., lower etching rates) of a Ta surface.

B. Ta etching rate reduction by surface oxidation

In Sec. III A, we conjectured that oxidation of a Ta surface enhanced its resistance against physical sputtering and an interaction of incident carbon with the Ta surface, if any, played little role on the reduction of its etching rate. To prove the conjecture, we performed experiments to clarify the effects of surface oxidation and physical sputtering only (without possible carbon effects), using Ar^+ and/or oxygen ion beams.

Figure 4 shows the etching rate of Ta by an ion beam generated from a mixture of Ar and O_2 gases and the thickness of a TaO_x layer formed on the Ta surface during the etching process as functions of the O_2-mixing ratio (denoted by X_{O_2}) of the ion beam source gas. The experiments were performed in the Ar/O_2 IBE system, which was discussed in Subsection II C. The ion beam energy was 500 eV, the ion current density to the sample was approximately 0.7 mA/cm^2, and the beam incident angle was normal to the sample surface. It is seen that the TaO_x thickness increases with X_{O_2} especially when X_{O_2} is larger than 2.5% and the Ta-etching rate rapidly decreases as the TaO_x thickness increases.

Figure 5 replots data of Fig. 4, showing the correlation between the etching rate and the TaO_x layer thickness. It is seen that the etching rate decreases monotonically with the TaO_x thickness and, for example, the etching rate of Ta covered with a 3.7 nm thick oxide layer is shown to be about 1/50 of that of metallic Ta (i.e., Ta with no oxide layer, TaO_x thickness = 0 nm).

Negative correlations between the metal etching rate and oxide formation, similar to those shown in Fig. 4, were also reported for Mo and Ti by Ar^+ ion sputtering with oxygen by Abe and Yamashina.[33] It was claimed in their study that the reduction of the sputtering rates was caused by the formation of oxide layers on the metal surfaces.

FIG. 5. Correlation between the Ta etching rate and the oxide thickness formed during the ion beam etching process shown in Fig. 4. The vertical axis is in the logarithmic scale.

C. Etching characteristics of Ta_2O_5

In this subsection, we examine the etching characteristics of Ta_2O_5 as we surmise that Ta_2O_5 is much more resistant against physical sputtering than metallic Ta; in other words, the etching rate of Ta_2O_5 is much lower than that of metallic Ta. Figure 6 shows the etching rate of Ta_2O_5 by an ion beam generated from a mixture of Ar and O_2 gases as functions of the O_2-mixing ratio X_{O_2} of the ion beam source gas. The experiments were performed in the Ar/O_2 IBE system, as those in Fig. 4. The ion beam energy was 500 eV, the ion current density to the sample was approximately 0.7 mA/cm^2, and the beam incident angle was normal to the sample surface.

It is seen in Fig. 6 that, contrary to the surmise, the etching rate of Ta_2O_5 by Ar^+ ion irradiation (35 nm/min) is
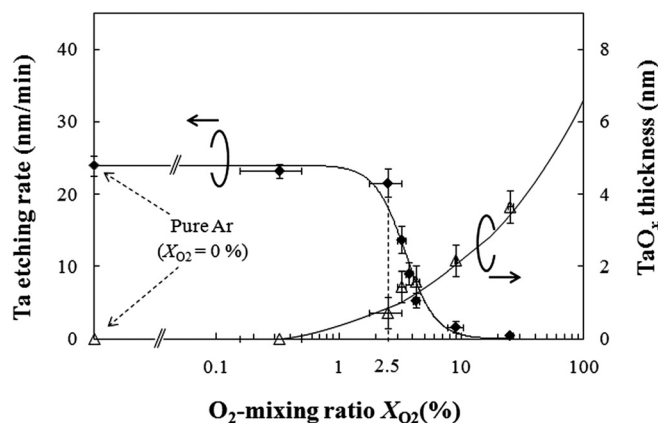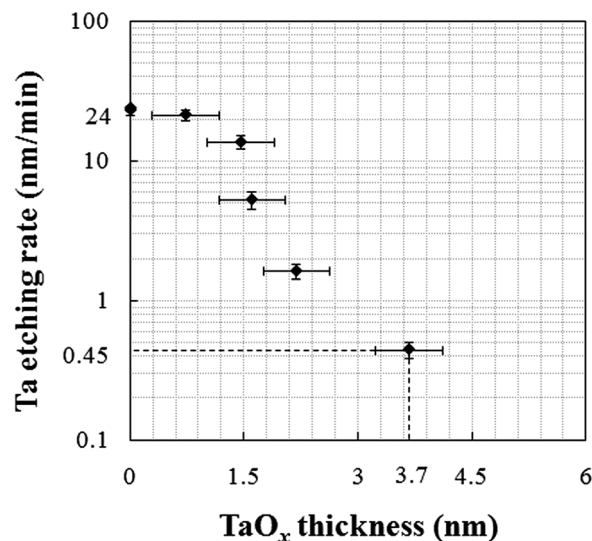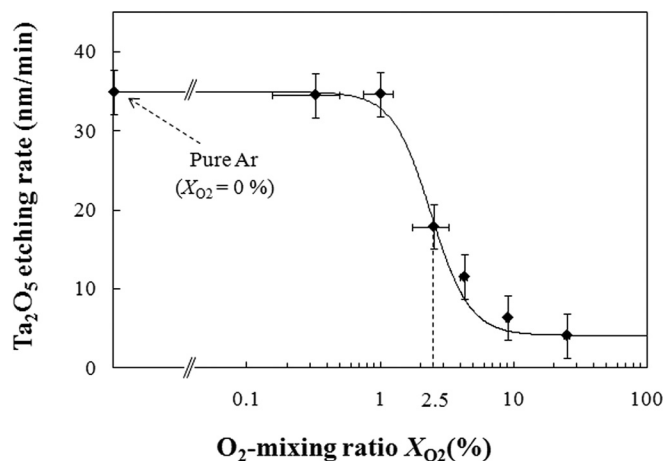

FIG. 4. Etching rate of Ta by an ion beam generated from a mixture of Ar and O_2 gases and the thickness of a TaO_x layer formed on the Ta surface during the etching process as functions of the O_2-mixing ratio X_{O_2} of the ion beam source gas. The experiments were performed in the Ar/O_2 IBE system. The thickness of the oxide layer plotted here is the one when the sample is exposed to the ion beam for 50 s. The ion beam energy is 500 eV, the ion current density to the sample is approximately 0.7 mA/cm^2, and the beam incident angle is normal to the sample surface.

FIG. 6. Etching rate of Ta_2O_5 by an ion beam generated from a mixture of Ar and O_2 gases as a function of the O_2-mixing ratio X_{O_2} of the ion beam source gas. The experiments were performed in the Ar/O_2 IBE system. The ion beam energy is 500 eV, the ion current density to the sample is approximately 0.7 mA/cm^2, and the beam incident angle is normal to the sample surface.

higher than that of Ta given in Fig. 4 (i.e., 24 nm/min). However, it should be noted that the density of Ta_2O_5 (typically 8.73 g/cm^3) is nearly half of that of Ta (16.69 g/cm^3) and the results are consistent with the sputtering yield data of Ta and Ta_2O_5 by Ar$^+$ ion irradiation given in Ref. 24, which shows that the sputtering yield of Ta is larger than that of Ta_2O_5. It should be also noted that the sputtering yield of Ta_2O_5 decreases significantly as X_{O_2} increases, or the oxygen content increases, which suggests that the chemical compositions of the Ta_2O_5 surface subject to Ar$^+$ ion bombardment may not be the same as those of true Ta_2O_5.

Figure 7 shows the narrow XPS scan spectra of Ta4f and O1s of a Ta_2O_5 surface subject to a pure Ar$^+$ ion beam at different times. The Ta_2O_5 sample here was irradiated by an Ar$^+$ ion beam emitted from an Ar ion gun equipped in a standard stand-alone XPS system, not in the Ar/O$_2$ IBE system used for the experiments shown in Fig. 6. The Ar$^+$ ion beam was 1 keV with a current density of 12.5 μA/cm^2. The beam incident angle was 45° to the sample surface.

It is clearly seen in Fig. 7 that the oxidation states of Ta shown in the Ta4f spectra shift toward lower values and the intensity of the O1s peak decreases as the beam irradiation time increases. Similar results have been reported for Ta_2O_5

etching by Ar$^+$ ion beams by Hashimoto *et al.*[34] The results indicate that oxygen of a Ta_2O_5 surface is preferentially sputtered by incident Ar$^+$ ions and the Ta_2O_5 surface becomes more metallic, meaning that it contains more Ta atoms with lower oxidation states than the initial Ta_2O_5 surface.

Figure 8 shows the ratio of the atomic concentration of O to that of Ta on the Ta_2O_5 surface irradiated by a 1 keV Ar$^+$ ion beam as a function of the beam irradiation time. The data were obtained from the same series of experiments as those shown in Fig. 7 at multiple time instances, calculated from the narrow scan spectra of the sample for Ta4f and O1s. It is clearly seen that oxygen is preferentially sputtered by incident Ar$^+$ ions.

The removal of oxygen from a Ta_2O_5 surface by Ar$^+$ ion physical sputtering is also observed from SIMS spectra obtained from experiments performed in the Ar/O$_2$ IBE system. Figure 9 shows time evolution of secondary ion intensities from the Ta_2O_5 surfaces when they are irradiated by (a) a pure Ar ion beam ($X_{O_2} = 0\%$) and (b) an ion beam formed from an Ar and O$_2$ mixture gas ($X_{O_2} = 25\%$). The incident beam energy is 500 eV, and the beam incident angle is normal to the sample surface. One should note that the ion
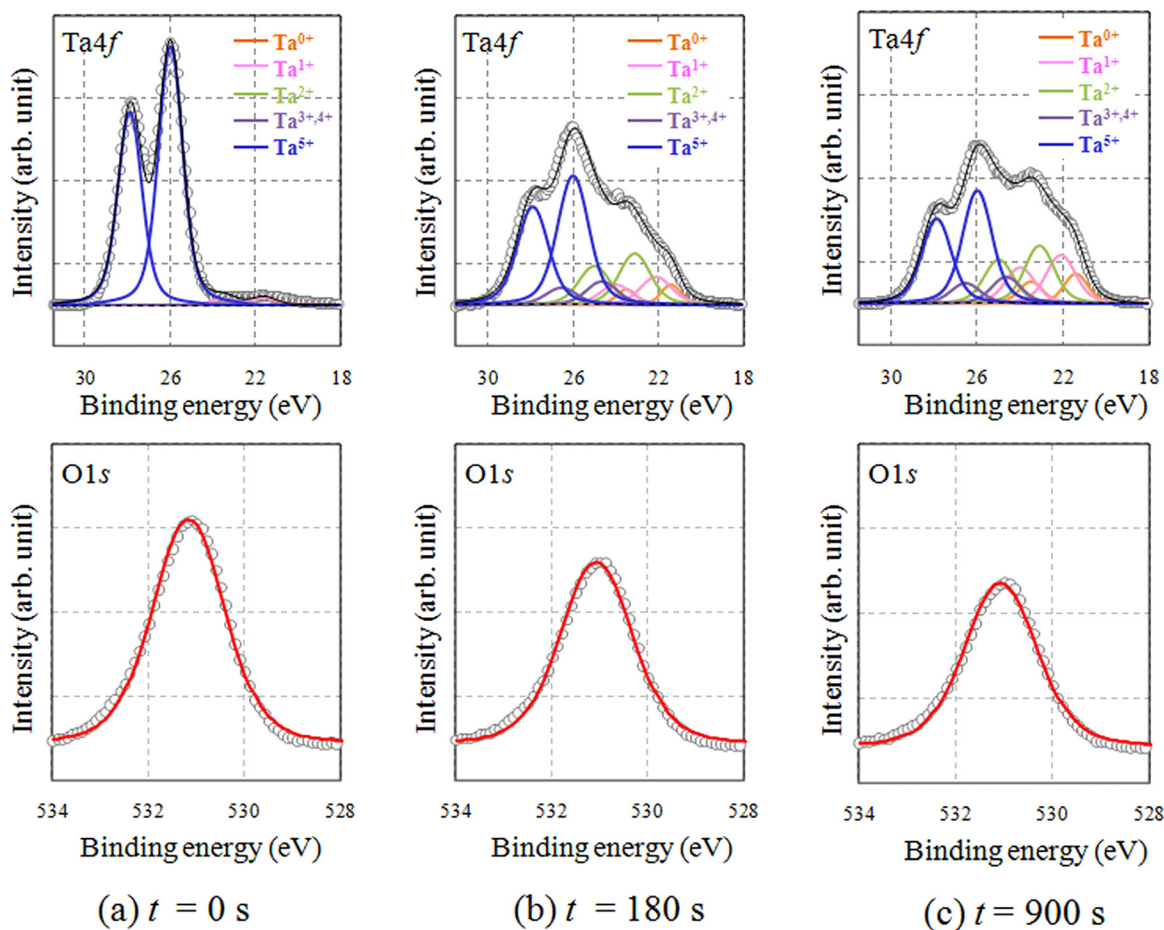

FIG. 7. (Color online) Narrow XPS scan spectra of Ta_2O_5 at different Ar$^+$ ion irradiation time t. The experiments were performed in a standard stand-alone XPS system equipped with an Ar ion gun, where a Ta_2O_5 sample was placed and irradiated by a 1 keV Ar$^+$ ion beam with a current density of 12.5 μA/cm^2. The beam incident angle is 45° to the sample surface.
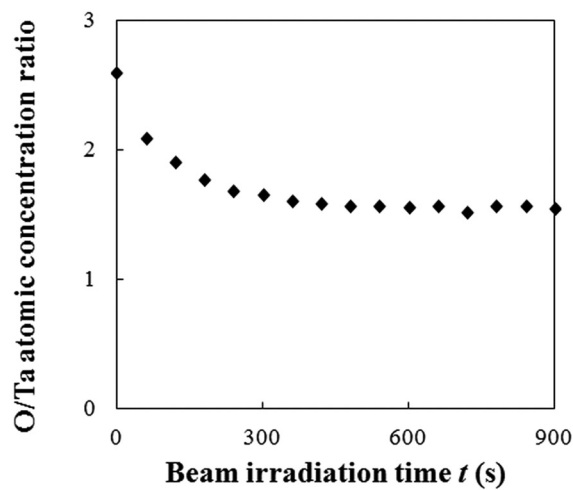
FIG. 8. Ratio of atomic concentrations of O and Ta of a Ta_2O_5 surface irradiated by a 1 keV Ar^+ ion beam as a function of the ion irradiation time. The experimental conditions are the same as those of Fig. 7. The ratio was calculated from the narrow scan spectra of Ta4f and O1s such as those given in Fig. 7. It is seen that oxygen is preferentially sputtered by Ar^+ ion beam irradiation.

beam energy and current density of the Ar/O_2 IBE system were different from those of the Ar ion gun in the standard stand-alone XPS system, so that the time scales (i.e., horizontal axes) of Figs. 8 and 9 may not be directly compared. It is seen in Fig. 9(a) that the TaO^+ and TaO_2^+ intensities increase to significant levels initially and then rapidly decrease to lower values as the beam irradiation continues, indicating that the amount of oxygen on the Ta_2O_5 surface is reduced by Ar^+ ion bombardment. Figure 9(b) shows, on the other hand, that the TaO^+ and TaO_2^+ intensities remain at approximately constant values from the initial stage, indicating that the surface chemical compositions (and therefore the oxidation states) of the Ta_2O_5 film also remains unchanged because of a sufficient supply of oxygen from the incident beam.

D. Discussion of etching resistance of a Ta mask

As seen in Figs. 7 and 9, oxygen of Ta_2O_5 is preferentially sputtered from the surface by Ar^+ ion bombardment at an incident energy of 500 eV–1 keV. Therefore, what seems an etching of Ta_2O_5 by energetic Ar^+ ions is actually an etching of a surface with more metallic Ta and suboxides (i.e., TaO_x with $x < 2.5$) rather than pure Ta_2O_5. Accordingly, the etching rate of such a surface is closer to that of Ta. Both Figs. 4 and 6 show that, as we increase the oxygen content of the incident ion beam, the etching rates of both Ta and Ta_2O_5 decrease to significantly low values. Since no *in situ* XPS is available in the Ar/O_2 IBE system, we have no direct evidence showing that the oxidation states of Ta or Ta_2O_5 surface is higher with higher oxygen content in the incident ion beam. However, as shown in Figs. 6 and 9, if more oxygen is supplied to a Ta_2O_5 surface as part of incident ions, more oxygen is incorporated into the surface and bonded with Ta. Therefore, a higher supply of oxygen to a Ta or Ta_2O_5 surface is also likely to increase the oxidation states of surface Ta, compensating oxygen loss by physical sputtering. Based on these observations, we conclude that the etching rate of tantalum oxide with a higher oxidation state is much lower than that of Ta.

It may be of interest to note that the etching rate of Ta at high O_2 mixing ratio X_{O_2} is much lower than that of Ta_2O_5, as shown in Figs. 4 and 6. This seems contradictory to what we have claimed; i.e., that, with a sufficiently high oxygen supply, a similar oxide film with high oxidation states should be formed on either a Ta or Ta_2O_5 surface and therefore their etching rates should be essentially the same. We postulate that this is caused by fast oxidation of metallic Ta as well as volume difference between Ta and its oxide (especially Ta_2O_5). When a supply of oxygen to the surface is sufficiently high (e.g., $X_{O_2} > 10\%$ in Fig. 4), an oxide layer is formed on a Ta surface, which is quickly removed by incident ion beam, but the removal of the oxide layer is balanced by its formation. On the other hand, when oxygen is preferentially removed from Ta_2O_5 and the surface becomes more
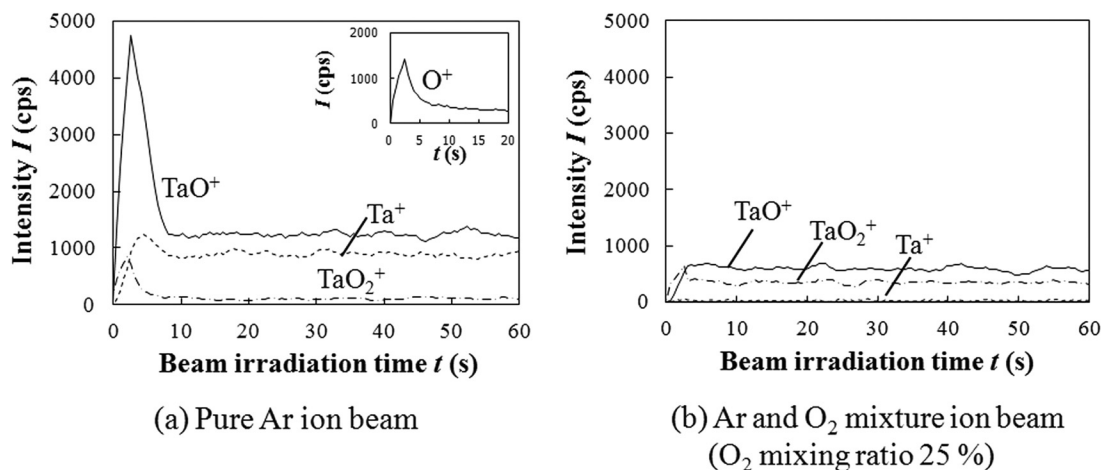

(a) Pure Ar ion beam

(b) Ar and O_2 mixture ion beam
(O$_2$ mixing ratio 25 %)

FIG. 9. Intensities of secondary ions emitted from a Ta_2O_5 surface by (a) a pure Ar-ion beam ($X_{O_2} = 0\%$) and (b) an ion beam from a mixture of Ar and O_2 gas ($X_{O_2} = 25\%$) as functions of the beam irradiation time. The experiments were performed in the Ar/O_2 IBE system. The inset in (a) shows the intensity of O^+ secondary ions. The intensity of O^+ secondary ions in (b) was below the detection limit. The ion beam energy is 500 eV, the ion current density to the sample is approximately 0.7 mA/cm^2, and the beam incident angle is normal to the sample surface.

metallic Ta, the volume of TaO_x decreases (and the depth increases) significantly even if no Ta is removed from surface. More detailed discussion on the balance between the formation and removal of an oxide layer by ion bombardment, which may need to be quantitatively analyzed with some reaction models, is beyond the scope of the present study and deferred to future work.

Angular dependence of the Ta etching rate given in Fig. 2 may also be accounted for by a similar argument on the negative correlation between the etching rate and the surface oxidation. The low etching rate of Ta at a low CO^+ ion irradiation angle may be caused by the formation of an oxide later with higher oxidation states whereas the high etching rate at a relatively large angle of ion incidence is caused by less surface oxidation. Although we have not examined closely why the surface oxidation varies with the ion irradiation angle, we conjecture that the surface oxidation states are determined by the balance between oxygen incorporation from the incident beam into the surface and preferential sputtering of oxygen from the surface by physical sputtering. The rate of oxygen incorporation into the surface, i.e., sticking coefficient or deposition rate of incident oxygen, is likely to vary with the ion incident angle if oxygen is supplied as energetic ions. It is known that incident ions with an oblique angle of incidence are more likely to be reflected from the surface than those of normal incidence. Detailed analyses of surface oxidation processes by incident oxygen ions or atoms, including theoretical studies with molecular dynamics simulations,[35] are deferred to a future study.

IV. SUMMARY AND CONCLUSIONS

Motivated to understand the cause of strong dependence of the Ta etching rate by CO^+ ion irradiation on the incident angle, we have examined the correlation between the etching rate and its surface oxidation by energetic incident ion beams containing oxygen. As shown in Figs. 2 and 3, the etching rate of Ta by energetic CO^+ ions exhibits strong negative correlation with the oxidation states of the surface oxide layer formed during the etching process; the etching rate is lower when the oxidation states of the formed oxide layer is higher.

Figures 4 and 5 also clearly show the direct correlation between the Ta etching rate and the thickness of the formed oxide layer in etching processes with oxygen-containing ion beams. For example, it is shown in this study that the etching rate of Ta covered with a 3.7 nm thick oxide layer is shown to be about 1/50 of that of metallic Ta. The XPS and SIMS studies shown in Figs. 7–9 indicate that, when a Ta_2O_5 surface is subject to physical sputtering by energetic Ar^+ ions, its surface oxygen is more readily sputtered away and the surface becomes more metallic. The SIMS studies also show that, if more oxygen is supplied to a Ta_2O_5 surface as part of incident ions, more oxygen is incorporated into the surface and bonded with Ta, which suggests that the oxidation states of Ta increase with the oxygen supply.

Thus, it has been found that the dry etching resistance of Ta is highly correlated with the oxidation states of Ta in the surface oxide layer formed by ion irradiation; the higher the

oxidation states are, the lower the etching rate of Ta covered with an oxide layer becomes. It has also been shown that the angular dependence of the etching rate of Ta by CO^+ ion irradiation and that of the surface oxidation states of Ta are highly correlated. We thus conjecture that the strong angular dependence of the Ta etching rate with CO^+ ion irradiation is caused by the angular dependence of the surface oxidation states. Although we have not yet clarified how the oxidation states of the formed oxide layer depend on the irradiation angle of the oxygen-containing ion beam, the oxidation states must be determined by the balance between oxygen incorporation into the surface and preferential sputtering of oxygen by ion irradiation. Detailed analyses of such a balance are deferred to a future study.

[1]G. Muller, T. Happ, M. Kund, G. Y. Lee, N. Nagel, and R. Sezi, *IEDM Technical Digest* (IEEE, San Francisco, CA, 2004), pp. 567–570.

[2]T. M. Maffitt, J. K. DeBrosse, J. A. Gabric, E. T. Gow, M. C. Lamorey, J. S. Parenteau, D. R. Willmott, M. A. Wood, and W. J. Gallagher, IBM J. Res. Dev. **50**, 25 (2006).

[3]S. Yuasa, T. Nagahama, A. Fukushima, Y. Suzuki, and K. Ando, Nat. Mater. **3** 868 (2004).

[4]S. S. P. Parkin, C. Kaiser, A. Panchula, P. M. Rice, B. Hughes, M. Samant, and S.-H. Yang, Nat. Mater. **3**, 862 (2004).

[5]H. Kubota *et al.*, Jpn. J. Appl. Phys. **44**, L 1237 (2005).

[6]M. Hosomi *et al.*, *IEDM Technical Digest* (IEEE, Washington, DC, 2005), pp. 459–462.

[7]J. Hayakawa *et al.*, IEEE Trans. Magn. **44**, 1962 (2008).

[8]S. Ikeda *et al.*, Nat. Mater. **9**, 721 (2010).

[9]I. Nakatani, IEEE Trans. Magn. **32**, 4448 (1996).

[10]K. B. Jung, J. Hong, H. Cho, S. Onishi, D. Johnson, Y. D. Park, J. R. Childress, and S. J. Pearton, J. Vac. Sci. Technol. A **17**, 535 (1999).

[11]K. B. Jung *et al.*, J. Appl. Phys. **85**, 4788 (1999).

[12]N. Matsui, K. Mashimo, A. Egami, A. Konishi, O. Okada, and T. Tsukada, Vaccum **66**, 479 (2002).

[13]H. Kubota, K. Ueda, Y. Ando, and T. Miyazaki, J. Magn. Magn. Mater. **272–276**, e1421 (2004).

[14]Y. Otani, H. Kubota, A. Fukushima, H. Maehara, T. Osada, S. Yuasa, and K. Ando, IEEE Trans. Magn. **43**, 2776 (2007).

[15]J.-Y. Park, S.-K. Kang, M.-H. Jeon, M. S. Jhon, and G.-Y. Yeom, J. Electrochem. Soc. **158**, H1 (2011).

[16]E. H. Kim, T. Y. Lee, and C. W. Chung, J. Electrochem. Soc. **159**, H230 (2012).

[17]M. Lee and W.-J. Lee, Appl. Surf. Sci. **258**, 8100 (2012).

[18]M. H. Jeon, H. J. Kim, K. C. Yang, S. K. Kang, K. N. Kim, and G. Y. Yeom, Jpn. J. Appl. Phys. **52**, 05EB03 (2013).

[19]K. Karahashi, T. Ito, and S. Hamaguchi, Proc. Int. Symp. Dry Process **33**, A-6 (2011).

[20]Y. Yamamura and H. Tawara, At. Data Nucl. Data **62**, 149 (1996).

[21]S. Hamaguchi, M. Dalvie, R. T. Farouki, and S. Sethuraman, J. Appl. Phys. **74**, 5172 (1993).

[22]S. Hamaguchi and M. Dalvie, J. Electrochem. Soc. **141**, 1964 (1994).

[23]S. Hamaguchi, A. A. Mayo, S. M. Rossnagel, D. E. Kotecki, K. R. Milkove, C. Wang, and C. E. Farrell, Jpn. J. Appl. Phys. **36**, 4762 (1997).

[24]H. Li, Y. Muraki, K. Karahashi, and S. Hamaguchi, J. Vac. Sci. Technol. A **33**, 040602 (2015).

[25]K. Ishikawa, K. Karahashi, H. Tsuboi, K. Yanai, and M. Nakamura, J. Vac. Sci. Technol. A **21**, L1 (2003).

[26]K. Karahashi, K. Yanai, K. Ishikawa, H. Tsuboi, K. Kurihara, and M. Nakamura, J. Vac. Sci. Technol. A **22**, 1166 (2004).

[27]K. Yanai, K. Karahashi, K. Ishikawa, and M. Nakamura, J. Appl. Phys. **97**, 053302 (2005).

[28]T. Ito, K. Karahashi, M. Fukasawa, T. Tatsumi, and S. Hamaguchi, Jpn. J. Appl. Phys. **50**, 08KD02 (2011).

[29]T. Ito, K. Karahashi, M. Fukasawa, T. Tatsumi, and S. Hamaguchi, J. Vac. Sci. Technol. A **29**, 050601 (2011).

[30]T. Ito, K. Karahashi, K. Mizotani, M. Isobe, S.-Y. Kang, M. Honda, and S. Hamaguchi, Jpn. J. Appl. Phys. **51**, 08HB01 (2012).

[31]T. Ito, K. Karahashi, S.-Y. Kang, and S. Hamaguchi, J. Vac. Sci. Technol. A **31**, 031301 (2013).

[32]K. Karahashi and S. Hamaguchi, J. Phys. D Appl. Phys. **47**, 224008 (2014).

[33]T. Abe and T. Yamashina, Thin Solid Films **30**, 19 (1975).

[34]S. Hashimoto, C. Tanaka, A. Murata, and T. Sakurada, J. Surf. Anal. **13**, 14 (2006).

[35]K. Mizotani, M. Isobe, K. Karahashi, and S. Hamaguchi, "Numerical simulation of atomiclayer oxidation of silicon by oxygen gas cluster beams," Plasma Fusion Res. (in press).